ELSEVIER

2-(1-Isopropyl-2-benzimidazolyl)-6-(1-aryliminoethyl)pyridyl transition metal (Fe, Co, and Ni) dichlorides: Syntheses, characterizations and their catalytic behaviors toward ethylene reactivity

Yanjun Chen [a,b], Peng Hao [b], Weiwei Zuo [b], Kun Gao [a,*], Wen-Hua Sun [a,b,*]

[a] State Key Laboratory of Applied Organic Chemistry, College of Chemistry and Chemical Engineering, Lanzhou University, Lanzhou 730000, China
[b] Key Laboratory of Engineering Plastics, Beijing National Laboratory for Molecular Sciences, Institute of Chemistry, Chinese Academy of Sciences, Beijing 100080, China

Abstract

A series of 2-(1-isopropyl-2-benzimidazolyl)-6-(1-aryliminoethyl)pyridyl metal complexes [iron (II) (**1a–6a**), cobalt (II) (**1b–6b**) and nickel (II) (**1c–6c**)] were synthesized and fully characterized by elemental and spectroscopic analyses. Single-crystal X-ray diffraction analyses of five coordinated complexes **5a**, **3b**, **5b**, **1c** and **2c** reveal **5a** and **5b** as distorted trigonal-bipyramidal geometry, and **3b**, **1c** and **2c** as distorted square pyramidal geometry. All complexes performed ethylene reactivity with the assistance of various organoaluminums. The iron complexes displayed good activities in the presence of MAO and MMAO. Upon activated by Et$_2$AlCl, the cobalt analogues showed moderate ethylene reactivity, while the nickel analogues exhibited relatively higher activities.
© 2008 Elsevier B.V. All rights reserved.

Keywords: Transition metal complex; Iron; Cobalt; Nickel; 2-(Benzimidazolyl)-6-iminopyridine; Ethylene reactivity

1. Introduction

Ethylene oligomerization presents one of the major industrial processes for the production of linear α-olefins in the range of C$_6$–C$_{20}$ with annual millions of tons productivities [1–3]. α-Olefins are fundamental substances amongst manufactures of detergents, synthetic lubricants and plasticizer alcohol and some co-polymers. Originally linear α-olefins were manufactured by the Ziegler (Alfen) process in the presence of TEA (triethylaluminum). Later on, the catalytic system employing nickel complex was developed as famous SHOP process [4]. Along with exploring new transition metal complexes as catalysts for ethylene polymerization [5], the great progress has been made for ethylene oligomerization due to the same reaction concept of ethylene oligomerization and polymerization. The past decade witnessed the discovery of numerous models of transition metal complexes as catalysts, in which the most famous model has been focused on metal complexes bearing 2,6-bis(imino)pyridines initially developed by the groups of Brookhart [6] and Gibson [7]. Beyond following works regarding to this model [8], the alternative models of heterocyclic compounds providing three-nitrogen in coordination have been developed in our group [5h]. Those interesting complexes with good to high activities in ethylene reactivity contain newly developed ligands such as 2-imino-1,10-phenanthroline derivatives (**A**, Scheme 1) [9], *N*-((pyridin-2-yl)methylene)-quinolin-8-amine derivatives
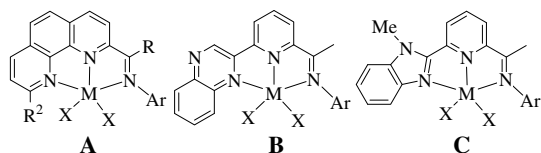
Scheme 1. Highly effective catalysts of newly N_3-tridentate metal complexes.

	1	2	3	4	5	6
R^1	Me	Et	^iPr	Cl	Me	Me
R^2	H	H	H	H	Me	Br

1a-6a: M=Fe;
1b-6b: M=Co;
1c-6c: M=Ni.

Scheme 2. Synthesis of metal complexes.

[10], 2-quinoxalinyl-6-iminopyridines (**B**, Scheme 1) [11], and recently 2-(1-methyl-2-benzimidazolyl)-6-(1-aryl iminoethyl)pyridines (**C**, Scheme 1) [12]. With those model complexes, the further modifications have been progressing along with finding optimum catalytic conditions.

In our extensive research of model catalyst **C** containing 2-(1-methyl-2-benzimidazolyl)-6-(1-aryliminoethyl)pyridines [12], 2-(1-isopropyl-2-benzimidazolyl)-6-(1-aryliminoethyl) pyridines have been synthesized and used to form chromium complexes as catalysts for ethylene reactions [13]. The substantive and systematic research includes transition metals such as iron, cobalt, nickel, etc. In comparison of their analogues ligated by 2-(1-methyl-2-benzimidazolyl)-6-(1-aryliminoethyl)pyridines, the titled complexes with isopropyl instead of methyl group are expected to be more soluble and more active. The titled complexes were synthesized and characterized in detail; moreover, their molecular structures of complexes **5a**, **3b**, **5b**, **1c** and **2c** were confirmed by single-crystal X-ray diffraction. In the presence of suitable organoaluminums, these complexes showed moderate to good catalytic activities toward ethylene oligomerization and polymerization for oligomers and polyethylene wax. The effects of substituents on the ligands, cocatalysts, the Al/metal molar ratio, and reaction temperature on their catalytic activities and selectivities have been investigated in detail. Herein, the syntheses and characterizations of the titled complexes are reported along with their catalytic performances towards ethylene oligomerization and polymerization.

2. Results and discussion

2.1. Synthesis and characterization

The syntheses and characterizations of organic compounds used as ligands were reported in our previous paper [13], in addition, the new 4-bromo-*N*-(1-(6-(1-isopropyl-1*H*- benzo[*d*]imidazol-2-yl)pyridin-2-yl)ethylidene)-2,6-dimethylbenzenamine was prepared in the same manner through the condensation reaction of 2-(1-isopropyl-2-benzimidazolyl)-6-acetylpyridine and 4-bromo-2,6-dimethylaniline.

According to the literature method, all titled complexes were formed in good to high yields. The iron (II) complexes **1a–6a** were easily prepared by mixing the corresponding ligands and 1 equiv. of $FeCl_2 \cdot 4H_2O$ in ethanol at room temperature under nitrogen (Scheme 2). The complexes were precipitated from the reaction solutions as blue pow
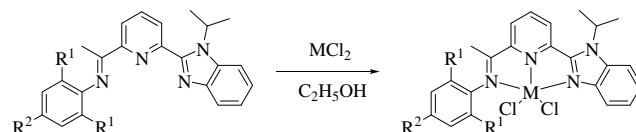
ders, separated by filtration, washed with diethyl ether and dried in vacuum as air-stable compounds with good purity in yields (80–99%). The complexes were characterized by FT-IR spectra and elemental analyses. In the IR spectra of these iron (II) complexes, the stretching vibration bands of the C=N groups apparently shifted to lower wave number (1591–1599 cm^{-1}) with greatly reduced intensity, compared with the corresponding ligands (1643–1658 cm^{-1}) [13], indicating the coordination interaction between the imine nitrogen atom and the metal cation. In addition, the molecular structure of **5a** was confirmed by the single-crystal X-ray diffraction analysis.

Using the same synthetic method (Scheme 2), the cobalt analogues (**1b–6b**) were successfully prepared and characterized by FT-IR spectra and elemental analyses. The lower frequencies of C=N bonds (1591–1593 cm^{-1}) in complexes indicated effective coordination of the imine nitrogen atom to the cobalt one. The molecular structures of **3b** and **5b** were determined by single crystal X-ray diffraction analyses. Similarly, their nickel analogues (**1c–6c**) were prepared (Scheme 2) and carefully characterized. Moreover, the molecular structures of **1c** and **2c** were further determined by single crystal X-ray diffraction analyses.

2.2. Molecular structures

Single crystals of complex **5a** suitable for X-ray diffraction analysis were obtained by slow diffusion of diethyl ether into its methanol solution under nitrogen. The asymmetric unit of complex **5a** contains the halves of two independent molecules, as shown in Fig. 1; and the poor structural quality might be the cause for $R_1 = 0.0998$. The coordination geometry around the iron center can be described as a distorted trigonal-bipyramidal in which one nitrogen atom N(2) of pyridyl ring and two chlorine atoms (Cl(1), Cl(2)) form the equatorial plane, which is similar to their iron analogue complexes ligated by 2-(1-methyl-2-benzimidazole)-6-(1-aryliminoethyl)pyridines [12a]. The two independent molecules have slightly different bond lengths and bond angles, as shown in Table 1. In molecule (**5a**-1), the iron center slightly deviates by 0.0295 Å from the triangular plane formed by N(2), Cl(1) and Cl(2), while this deviation is 0.0058 Å in molecule (**5a**-2). Furthermore, differences are observed for the dihedral angles between the equatorial plane and the pyridyl one, the imino-aryl ring and the pyridyl ring (91.4° and 84.7° in (**5a**-1) vs. 80.3° and 75.9° in (**5a**-2)). In (**5a**-1), the plane of the chelating
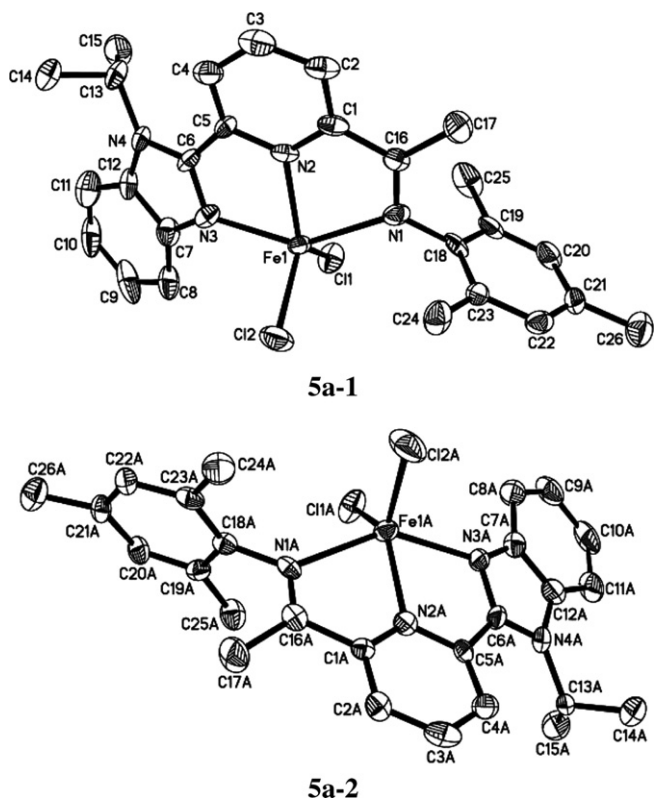
Fig. 1. Crystal structure of complex **5a** showing the two independent molecules of the asymmetric unit. Thermal ellipsoids are shown at 30% probability; hydrogen atoms and solvent have been omitted for clarity.

Table 1
Selected bond lengths (Å) and angles (°) for complex **5a**

Bond lengths (Å)			
Fe(1)–N(1)	2.309(9)	Fe(1A)–N(1A)	2.307(8)
Fe(1)–N(2)	2.154(7)	Fe(1A)–N(2A)	2.115(7)
Fe(1)–N(3)	2.160(8)	Fe(1A)–N(3A)	2.209(7)
Fe(1)–Cl(1)	2.305(3)	Fe(1A)–Cl(1A)	2.281(3)
Fe(1)–Cl(2)	2.287(3)	Fe(1A)–Cl(2A)	2.294(3)
N(1)–C(16)	1.294(1)	N(1A)–C(16A)	1.269(1)
N(1)–C(18)	1.422(1)	N(1A)–C(18A)	1.444(1)
N(2)–C(1)	1.354(1)	N(2A)–C(1A)	1.344(1)
N(2)–C(5)	1.347(1)	N(2A)–C(5A)	1.324(1)
N(3)–C(6)	1.327(1)	N(3A)–C(6A)	1.313(1)
N(3)–C(7)	1.413(1)	N(3A)–C(7A)	1.379(1)
Bond angles (°)			
N(2)–Fe(1)–N(3)	73.1(3)	N(2A)–Fe(1A)–N(3A)	73.8(3)
N(2)–Fe(1)–N(1)	72.9(3)	N(2A)–Fe(1A)–N(1A)	72.7(3)
N(3)–Fe(1)–N(1)	145.5(3)	N(3A)–Fe(1A)–N(1A)	144.4(3)
N(2)–Fe(1)–Cl(1)	124.9(2)	N(2A)–Fe(1A)–Cl(1A)	131.2(2)
N(3)–Fe(1)–Cl(1)	96.3(2)	N(3A)–Fe(1A)–Cl(1A)	93.5(2)
N(1)–Fe(1)–Cl(1)	98.4(2)	N(1A)–Fe(1A)–Cl(1A)	99.50(2)
N(2)–Fe(1)–Cl(2)	120.1(2)	N(2A)–Fe(1A)–Cl(2A)	109.9(2)
N(3)–Fe(1)–Cl(2)	99.6(2)	N(3A)–Fe(1A)–Cl(2A)	104.9(2)
N(1)–Fe(1)–Cl(2)	102.1(2)	N(1A)–Fe(1A)–Cl(2A)	97.57(2)
Cl(1)–Fe(1)–Cl(2)	114.97(1)	Cl(1A)–Fe(1A)–Cl(2A)	118.88(2)

ring Fe(1)–N(3)–C(6)–C(5)–N(2)–C(1)–C(16)–N(1) is nearly perpendicular to both equatorial plane (89.3°) and the imino-aryl ring (91.9°), while the corresponding two dihedral angles deviated from 90° in (**5a**-2) (83.2(2)°,

85.4(3)°). In both molecules, the bond angles subtended by the axial Fe–N bonds are 145.5(3)° (N(1)–Fe(1)–N(3)) and 144.4(3)° (N(1A)–Fe(1A)–N(3A)), respectively. The Fe–N bond in the equatorial plane in each molecule is clearly shorter than the two axial Fe–N bonds, and the axial Fe–N (N from the imidazole ring) bond is shorter than the Fe–N_{imino} one. The two Fe–Cl bond lengths are similar in each molecular structure. Although the two imino C=N bonds are slightly different (1.294(1) Å in (**5a**-1) and 1.269(1) Å in (**5a**-2)), they are both typical imino C=N double bonds.

Single crystals of cobalt complexes **3b** and **5b** were grown by laying diethyl ether on their methanol solutions. The coordination geometry of complex **3b** could be described as a distorted square pyramidal, while the coordination geometry of complex **5b** is a distorted trigonal-bipyramidal.

The molecular structure of **3b** is shown in Fig. 2, while selected bond lengths and angles are collected in Table 2. In the molecular structure of **3b**, the cobalt atom deviates by 0.4529 Å from the plane formed by N(1), N(2) and N(3), meanwhile the chlorine atom Cl(1) is almost in coplanar manner with deviation of 0.1729 Å, and the other chlorine atom Cl(2) deviates 2.1936 Å from this plane in the opposite direction. Based on this structural character, the coordination geometry of complex **3b** can be best described as a distorted square pyramidal with the basal plane composed by N(1), N(2), N(3) and Cl(1). This phenomenon is different from those of their analogue cobalt complexes, whose geometries around the cobalt center are trigonal-bipyramidal [12a].

The dihedral angle between the basal plane and the pyridine ring is 17.0°, while that between the basal plane and the benzimidazole ring is 12.5°. The imino-aryl ring is nearly perpendicular to the pyridine ring with the dihedral angle of 88.9°, so is the dihedral angle between the imino-aryl ring and the benzimidazole ring as 85.4°. The molecule
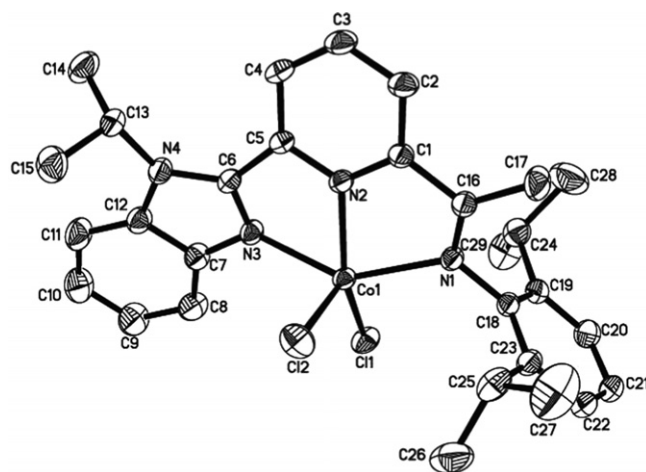
Fig. 2. Molecular structure of complex **3b**. Thermal ellipsoids are shown at 30% probability; hydrogen atoms and solvent have been omitted for clarity.

Table 2
Selected bond lengths (Å) and angles (°) for complexes **3b**

Bond lengths (Å)			
Co–N(1)	2.180(3)	Co–N(2)	2.079(3)
Co–N(3)	2.150(3)	Co–Cl(1)	2.2750(1)
Co–Cl(2)	2.2856(1)	N1–C(16)	1.284(5)
N1–C(18)	1.442(5)	N2–C(1)	1.334(5)
N2–C(5)	1.344(5)	N3–C(6)	1.332(5)
N3–C(7)	1.367(5)		

Bond angles (°)			
N(2)–Co–N(3)	74.88(1)	N(2)–Co–N(1)	74.83(1)
N(3)–Co–N(1)	144.56(1)	N(2)–Co–Cl(1)	151.44(1)
N(3)–Co–Cl(1)	99.55(1)	N(1)–Co–Cl(1)	98.27(9)
N(2)–Co–Cl(2)	93.72(9)	N(3)–Co–Cl(2)	97.04(1)
N(1)–Co–Cl(2)	102.85(1)	Cl(1)–Co–Cl(2)	114.83(5)

Table 3
Selected bond lengths (Å) and angles (°) for complex **5b**

Bond lengths (Å)			
Co(1)–N(1)	2.295(5)	Co(2)–N(5)	2.320(5)
Co(1)–N(2)	2.072(4)	Co(2)–N(6)	2.070(4)
Co(1)–N(3)	2.150(5)	Co(2)–N(7)	2.152(4)
Co(1)–Cl(1)	2.2718(2)	Co(2)–Cl(4)	2.2566(2)
Co(1)–Cl(2)	2.2724(2)	Co(2)–Cl(3)	2.274(2)
N(1)–C(16)	1.285(7)	N(5)–C(42)	1.282(7)
N(1)–C(18)	1.457(7)	N(5)–C(44)	1.437(7)
N(2)–C(1)	1.342(7)	N(6)–C(27)	1.349(7)
N(2)–C(5)	1.345(7)	N(6)–C(31)	1.350(6)
N(3)–C(6)	1.319(7)	N(7)–C(32)	1.324(7)
N(3)–C(7)	1.372(7)	N(7)–C(33)	1.412(7)

Bond angles (°)			
N(2)–Co(1)–N(3)	75.98(2)	N(6)–Co(2)–N(7)	75.94(2)
N(2)–Co(1)–N(1)	74.14(2)	N(6)–Co(2)–N(5)	73.33(2)
N(3)–Co(1)–N(1)	149.73(2)	N(7)–Co(2)–N(5)	147.25(2)
N(2)–Co(1)–Cl(1)	118.12(1)	N(6)–Co(2)–Cl(3)	108.26(2)
N(3)–Co(1)–Cl(1)	97.63(2)	N(7)–Co(2)–Cl(3)	104.11(1)
N(1)–Co(1)–Cl(1)	100.60(1)	N(5)–Co(2)–Cl(3)	96.05(1)
N(2)–Co(1)–Cl(2)	126.22(1)	N(6)–Co(2)–Cl(4)	132.26(1)
N(3)–Co(1)–Cl(2)	95.51(1)	N(7)–Co(2)–Cl(4)	94.72(1)
N(1)–Co(1)–Cl(2)	98.10(1)	N(5)–Co(2)–Cl(4)	97.55(1)
Cl(1)–Co(1)–Cl(2)	115.63(7)	Cl(3)–Co(2)–Cl(4)	119.37(9)

is asymmetric with slight difference of Co(1)–Cl(1) (2.2750(1) Å) and Co(1)–Cl(2) (2.2856(1) Å), and So three Co–N bond lengths as Co(1)–N(1) 2.180(3) Å, Co(1)–N(2) 2.079(3) Å and Co(1)–N(3) 2.150(3) Å, respectively. Those phenomena are similar to those in its chromium (III) analogue [13]. In addition, the N–Co–N angles are 74.83(1)°, 77.88(1)° and 144.56(1)°, which are smaller than those angles found in its chromium (III) analogues [13].

Unlike complex **3b**, however, the asymmetric unit of complex **5b** contains the halves of two independent molecules (Fig. 3). In the structure of complex **5b**, the two independent molecules give slightly different bond lengths and bond angles (Table 3). Both the coordination geometries

5b-1

5b-2

Fig. 3. Crystal structure of complex **5b** showing the two independent molecules of the asymmetric unit. Thermal ellipsoids are shown at 30% probability; hydrogen atoms and solvent have been omitted for clarity.

around the cobalt centers in these two molecules are distorted trigonal-bipyramidal due to the significant deviations of the chlorine atoms from the plane N(1)–N(2)–N(3) (1.6183 Å and 2.1936 Å in (**5b**-1), 1.1361 Å and 2.5314 Å in (**5b**-2), respectively). In molecule (**5b**-1), the cobalt center slightly deviates by 0.0233 Å from the triangular plane formed by N(2), Cl(1) and Cl(2), while this deviation is 0.0421 Å in molecule (**5b**-2). The dihedral angles are 89.3° and 95.0° in molecule (**5b**-1) between the equatorial plane and the pyridyl plane, and the imino-aryl ring and the benzimidazole ring, which are obviously different from the dihedral angles 80.5° and 82.1° in molecule (**5b**-2), respectively. In addition, the dihedral angles between the phenyl ring and the pyridyl ring are largely different as 94.2° in (**5b**-1) and 75.5° in (**5b**-2), respectively. In both molecules, the bond angles subtended by the axial Co–N bonds (149.73(2)° in (**5b**-1), and 147.25(2)° in (**5b**-2), respectively) are much wider than those of the iron analogue **5a** and cobalt analogue **3b**. In each molecule, the Co–N bond in the equatorial plane is shorter than that of the two axial Co–N bonds, which is agreeable with those of complexes **3b** and **5a**. In addition, the Co–N (imino) bond length of **5b** is obviously longer than that of complex **3b**. This effect is due to the introduction of the substituent at the *para*-position of the phenyl ring in **5b**.

Single crystals of nickel complexes **1c** and **2c** were obtained by slow diffusion diethyl ether into their corresponding methanol solutions. Similar to the structure of cobalt complex **3b**, the coordination geometries of **1c** and **2c** can be described as distorted square pyramidal with the basal plane composed by three coordination nitrogen atoms and one chlorine atom. In terms of reconsidering molecular structures of their analogues ligated by
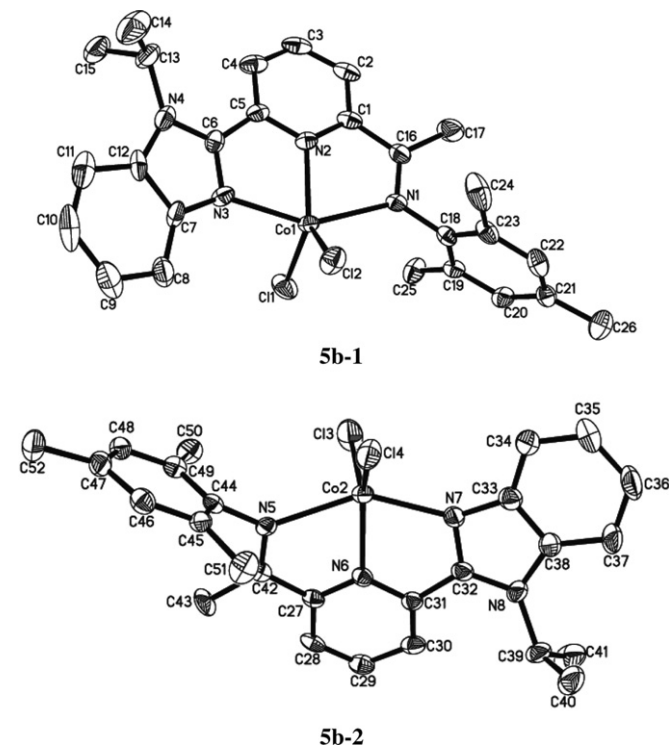
2-(1-methyl-2-benzimidazolyl)-6-(1-aryliminoethyl)pyridines [12b], those nickel complexes are also close to distorted square pyramidal geometry instead of distorted trigonal-bipyramidal (but it does not mean the previous express wrong to some extent with considering coordination geometry around nickel atom). Their molecular structures are shown in Figs. 4 and 5, respectively, and selected bond lengths and angles are collected in Table 4.

The central nickel atom in complex **1c** deviates by 0.2359 Å from the plane containing N(1), N(2), N(3), while the Cl(1) deviates by 0.5264 Å in the opposite direction. The basal plane composed by N(1), N(2), N(3) and Cl(1) is almost coplanar to the pyridyl ring with dihedral angle of 8.4°, and the pyridyl ring and the benzimidazole ring are also nearly coplanar with dihedral angle of 8.2°. The dihedral angles between the phenyl plane and the benzimidazole ring, and the phenyl plane with the pyridine ring are 78.0° and 84.7°, respectively. With the ligands containing the isopropyl group on benzimidazole ring instead of methyl one, slightly longer Ni–N bond (Ni–N(3)

Table 4
Selected bond lengths (Å) and angles (°) for complexes **1c** and **2c**

	1c	**2c**
Bond lengths (Å)		
Ni–N(1)	2.156(5)	2.166(3)
Ni–N(2)	2.006(5)	2.010(3)
Ni–N(3)	2.089(5)	2.089(2)
Ni–Cl(1)	2.2643(2)	2.2611(9)
Ni–Cl(2)	2.3129(2)	2.3147(1)
N1–C(16)	1.282(7)	1.280(4)
N1–C(18)	1.445(7)	1.445(4)
N2–C(1)	1.348(7)	1.338(4)
N2–C(5)	1.331(7)	1.345(4)
N3–C(6)	1.335(7)	1.333(4)
N3–C(7)	1.385(7)	1.384(4)
Bond angles (°)		
N(2)–Ni–N(3)	76.68(2)	76.89(1)
N(2)–Ni–N(1)	77.40(2)	76.81(1)
N(3)–Ni–N(1)	152.23(2)	149.97(1)
N(2)–Ni–Cl(1)	153.46(1)	157.81(8)
N(3)–Ni–Cl(1)	101.95(1)	101.34(8)
N(1)–Ni–Cl(1)	96.78(1)	97.56(8)
N(2)–Ni–Cl(2)	94.25(1)	92.13(8)
N(3)–Ni–Cl(2)	94.99(1)	96.97(8)
N(1)–Ni–Cl(2)	96.69(1)	98.22(8)
Cl(1)–Ni–Cl(2)	112.21(7)	109.99(4)

Fig. 4. Molecular structure of complex **1c**. Thermal ellipsoids are shown at 30% probability; hydrogen atoms and solvent have been omitted for clarity.
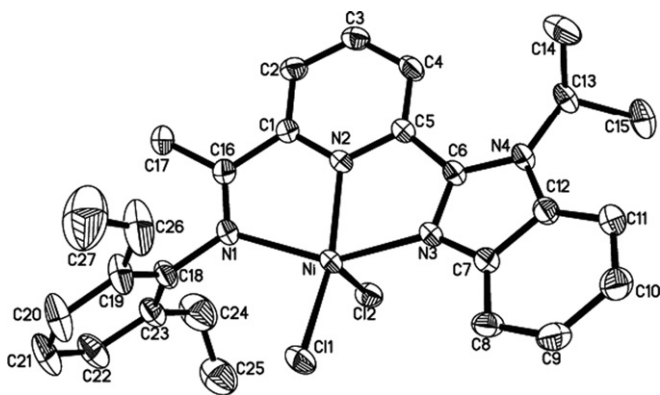
Fig. 5. Molecular structure of complex **2c**. Thermal ellipsoids are shown at 30% probability; hydrogen atoms and solvent have been omitted for clarity.

2.089(5) Å) is observed compared with the datum of its analogue with 2.0701(2) Å [12b], meanwhile slightly smaller angle N(1)–Ni–N(3) (152.23(2)°) and wider angle Cl(1)–Ni–Cl(2) (112.21(7)°) are observed than those angles in its analogue complex as 152.60(6)° and 110.17(2)°, respectively [12b]. In addition, the imino C=N bond still keeps distinctive double-bond character, and two Ni–Cl linkages show slightly differences, the Ni–Cl(1) being about 0.0486 Å shorter than that of Ni–Cl(2).

With ethyl instead of methyl of phenyl ring on imino group in complex **1c**, the molecular structure of complex **2c** (Fig. 5) is similar to that of complex **1c**, and its selected bond lengths and angles are listed in Table 4. In the molecular structure of **2c**, the nickel deviation (0.3417 Å) and the chlorine (Cl(1)) deviation (0.1403 Å) from the plane N(1)–N(2)–N(3) are slightly different to those in complex **1c**. The dihedral angle between the pyridine ring and the benzimidazole ring is 19.6° of complex **2c**, which is bigger than that of complex **1c** (8.2°). The difference of two Ni–Cl bond distances shows 0.0536 Å in complex **2c**, while the corresponding difference is 0.0486 Å in complex **1c**.

2.3. Catalytic behavior toward ethylene reactivity

2.3.1. Catalytic behavior of iron complexes

Various aluminum-based cocatalysts were used for exploring the catalytic activity of the iron complexes. Moderate to good activities were obtained with MAO and modified methylaluminoxane (MMAO) as cocatalysts. Complex **1a** was typically investigated under a range of reaction conditions, such as different cocatalysts, molar ratio of cocatalyst to iron and reaction temperature at

Table 5
Ethylene oligomerization and polymerization with **1a–6a**/MAO[a]

Entry	Compound	Al/Fe	P (atm)	T (°C)	K	Wax (g)	Activity[b]		Oligomer distribution[c]				
							Oligomer	Wax	$C_4/\sum C$	$C_6/\sum C$	$C_8/\sum C$	$\geqslant C_{10}/\sum C$	α-Olefin (%)
1	**1a**	200	10	20			0.02		100				>99
2	**1a**	500	10	20	0.52	Trace	1.52	Trace	29.2	23.2	14.7	32.9	>98
3	**1a**	1000	10	20	0.60	0.27	2.34	1.08	26.6	20.7	20.2	32.5	>98
4	**1a**	1500	10	20	0.55	0.13	1.31	0.52	31.3	22.6	14.7	31.4	>98
5	**1a**	1000	10	40	0.54	0.08.	1.28	0.32	28.7	22.9	17.6	30.8	>98
6	**1a**	1000	10	60	0.52	0.03	0.02	0.12	65.6	34.4			>99
7	**2a**	1000	10	20	0.43	0.10	1.62	0.40	49.4	26.0	11.1	13.5	>98
8	**3a**	1000	10	20	0.43	0.07	0.48	0.28	59.7	18.4	13.5	8.4	>98
9	**4a**	1000	10	20		Trace	0.02	Trace	100				>99
10	**5a**	1000	10	20	0.60	1.12	8.67	4.48	30.3	20.6	19.6	29.5	>98
11	**6a**	1000	10	20	0.61	0.04	3.01	0.16	26.0	20.5	18.8	34.7	>98
12	**5a**	1000	30	20	0.58	2.50	32.0	10.0	38.7	24.5	19.8	17.0	>98

[a] Reaction conditions: 5 μmol of catalyst; 10 atm of ethylene; 30 min; 100 mL of toluene.
[b] In units of 10^5 g (mol of Fe)$^{-1}$ h^{-1}.
[c] Determined by GC; $\sum C$ signifies the total amounts of oligomers.

10 atm of ethylene. Oligomers were predominant products. The detailed results are summarized in Table 5. The distribution of oligomers obtained in all cases resembles Schulz–Flory rules, which is characterized by the constant K, where K represents the probability of chain propagation (K = rate of propagation/((rate of propagation) + (rate of chain transfer) = (moles of C_{n+2})/(moles of C_n)) [14] and the K values are determined by the molar ratio of C_{14} and C_{12} fractions.

2.3.1.1. Ethylene activation in the presence of MAO. When MAO was employed as the cocatalyst and the Al/Fe molar ratio was changed from 200 to 1500, the catalytic activity of **1a** firstly increased and then decreased and displayed the maximum value at the Al/Fe molar ratio of 1000. With a fixed Al/Fe molar ratio of 1000 using MAO, the reaction temperature strongly affected the catalytic activity. The highest activity was obtained at 20 °C (Entry 3, Table 5). Higher reaction temperatures led to an obvious decrease in the catalytic activity (Entries 5 and 6, Table 5), most likely due to the decomposition of some active centers and the lower solubility of ethylene in toluene. It is well known that elevated ethylene pressure promotes higher activities; this phenomenon was also observed with the iron catalytic system. For **5a**/MAO system, its reactivity for oligomers and polymers were both enhanced sharply at 30 atm of ethylene pressure (Entry 12, Table 5).

To compare the effect of the ligand environments on the catalytic behaviors, all iron complexes **1a–6a** were investigated under the same conditions (Al/Fe molar ratio of 1000 and 20 °C). The 2,4,6-trimethyl-substituted complex **5a** performed the highest catalytic activity (Entry 10, Table 5). The variation of the R substituent on the phenyl ring of ligands resulted in changes of the catalytic performance. For complexes bearing alkyl substituents on the phenyl ring, it was observed that a decrease in steric hindrance of the R^1 group led to an enhanced activity with the order as **1a** > **2a** > **3a**. This observation was reversed in catalytic

systems of their analogues with MAO as cocatalyst [12a]. In addition, under the same conditions, the activity of its analogue 2-(1-methyl-2-benzimidazolyl)-6-(1-aryliminoethyl) pyridyliron complex [12a] was four times higher than that of complex **1a**. In fact, the titled complexes containing isopropyl substituted benzimidazole are commonly more soluble than their analogues containing methyl substituted benzimidazole [12a]. The negative influence might be caused by other factors. Previously it was concluded that the increase in net charge of metal center lowers the insertion barrier of ethylene to result in better catalytic activity in ethylene reaction with nickel systems [15]. The results in this work are consistent with this conclusion. The less catalytic activity than its analogue with methyl substituted benzimidazole was caused by the ligand with more electron-donating isopropyl substituent. The steric nature of the aromatic substituents may also make an influence on the activity. However, the substitution of two alkyl groups (complexes **1a**–**3a**) by two chloro groups (complex **4a**) in the *ortho*-positions leads to an almost inactive species (Entries 3 and 7–9, Table 5), which is in line with the results observed in their catalytic analogues [12a]. This looks totally different to the correlation between net charge of metal center and catalytic activity, however, un-monotonous relation of net charge and catalytic activity of iron (II) catalysts was obtained [16]. Therefore, further experimental and simulation researches are necessary for predicting catalytic activities of designing metal complexes as catalysts.

In addition, it seems that the substituent in the *para*-position of the imino-aryl group has a beneficial influence on the activity. The complexes **5a** and **6a**, which respectively bear an electron-donating methyl group and an electron-withdrawing bromo group in the *para*-position of the aryl ring, exhibited much higher activities than the corresponding complex **1a**. This is in agreement with the results observed for the chromium catalysts [13] and 2-quinoxalinyl-6-iminopyridyl iron catalysts [11b]. Furthermore,

catalyst **5a** with a less bulky and electron-donating substituent exhibited higher catalytic activity than catalyst **6a** with bromo group, which could be the combined results of the electronic and steric effects.

2.3.1.2. Ethylene activation in the presence of MMAO.

After routine selection of the ratio of MMAO to iron catalyst, good catalytic activity was observed at an Al/Fe molar ratio of 1000. Therefore, the catalytic behaviors of all tridentate iron complexes were investigated with a fixed Al/Fe molar ratio of 1000, and their results are summarized in Table 6. All the complexes displayed moderate catalytic activities for ethylene oligomerization with high α-olefin selectivity (>98%) at 10 atm of ethylene pressure. A noticeable effect of the alkyl substituents on the aryl ring can be observed. For catalysts bearing alkyl groups in the *ortho*-aryl positions, a reduction of steric bulk resulted in increased activity of the complexes. Hence, complex **1a** with methyl groups showed better activities of 5.96×10^5 g (mol of Fe)$^{-1}$ h^{-1} than complexes **2a** (with ethyl) and **3a** (with isopropyl) at 10 atm of ethylene. This followed the same tendency as the iron complexes with MAO as the cocatalyst discussed above, and such observations were also found in literature [17]. Similar to the result of system **1a**/MAO, under the same conditions, in the presence of MMAO, the activity of its analogue 2-(1-methyl-2-benzimidazolyl)-6-(1-aryliminoethyl) pyridyliron complex [12a] was two times higher than that of complex **1a**. In the presence of MMAO, the electronic effect on catalytic activity also followed the same tendency as the iron/MAO system. Complex **4a** with dichloro-phenyl group showed much lower activity than other catalysts. The introduction of electron-donating substituent in the *para*-position of the phenyl group resulted in increased activity (Entry 5, Table 6). Complex **5a**, which bears 2,4,6-trimethylphenyl group showed better catalytic activity than its analogues bearing 2,6-dialkylphenyl group (Entry 5 vs. Entries 1–3, Table 6). Additionally, complex **6a**, showed relatively lower activity than **5a** and comparable activity to its analogue complex **3a**, which demonstrated that the electron-withdrawing substituent in the *para*-position of the aryl ring had no obvious influence on the reactivity.

This phenomenon is different from what observed using MAO as the cocatalyst.

2.3.2. Ethylene oligomerization by cobalt and nickel complexes

The cobalt (II) complexes **1b**–**6b** were systematically investigated for the oligomerization of ethylene. When Et$_2$AlCl was used as cocatalyst, complex **1b** showed higher ethylene activity with high selectivity of α-olefins than those with MAO or MMAO as cocatalyst. The further detailed investigations were carried out with cocatalyst of Et$_2$AlCl, mainly producing butanes. It is notable that cobalt systems are less active than their iron analogues, and this is apparent for complexes ligated by bis(imino)pyridines [18] as well as other systems [19,20].

The influences of the Al/Co molar ratio and the reaction temperature on ethylene oligomerization were investigated in detail with complex **1b**. Variation of the Al/Co molar ratio from 400 to 900 significantly affected the oligomerization activity, and the optimum oligomerization activity was observed at the Al/Co molar ratio of 700. The catalytic performance of cobalt complex **1b** was greatly affected by the reaction temperature and the highest activity was observed at 30 °C (Entry 6, Table 7). In addition, increasing the temperature leads to a rapid decrease in the selectivity for α-olefins such as 97.5% at 20 °C and 86.6% at 60 °C (Entries 9–11, Table 7).

As shown in Table 7, the substituents of the ligands in the cobalt complexes significantly affect the catalytic activity of ethylene oligomerization. Among complexes **1b**–**3b**, **1b** with the methyl groups in the *ortho*-positions of the phenyl ring, showed the highest activity, and the activity decreased in the order **1b** (with substituent of dimethyl) > **2b** (with diethyl) > **3b** (with diisopropyl) under identical reaction conditions, but a little influence was observed on the selectivity of α-olefins. Complex **4b** bearing 2,6-dichlorophenyl group showed lower activity than its analogue **2b**, but better activity than **3b**. The same tendency was observed in the corresponding 2-(1-methyl-2-benzimidazolyl)-6-(1-aryliminoethyl)pyridylcobalt systems [12a]. The functional groups on the *para*-position of the phenyl ring in complexes **5b** and

Table 6
Ethylene oligomerization and polymerization with **1a**–**6a**/MMAO[a]

Entry	Compound	P (atm)	K	Wax (g)	Activity[b]		Oligomer distribution[c]				
					Oligomer	Wax	$C_4/\sum C$	$C_6/\sum C$	$C_8/\sum C$	$\geqslant C_{10}/\sum C$	α-Olefin (%)
1	**1a**	10	0.58	0.07	5.96	0.28	28.5	20.2	21.5	29.8	>98
2	**2a**	10	0.45	0.02	3.57	0.08	46.6	22.2	15.8	15.4	>98
3	**3a**	10		0.03	1.41	0.12	69.8	19.6	7.3	3.3	>98
4	**4a**	10		Trace	0.03	Trace	83.7	16.3			>99
5	**5a**	10	0.49	1.40	8.24	5.60	35.2	22.2	20.1	22.5	>98
6	**6a**	10	0.59	0.05	1.52	0.20	31.6	19.6	14.4	34.4	>98
7	**5a**	30	0.45	2.70	32.0	10.8	45.2	24.3	20.0	10.5	>98

[a] Reaction conditions: 5 μmol of catalyst; 10 atm of ethylene; 30 min; 20 °C; Al/Fe = 1000; 100 mL of toluene.
[b] In units of 10^5 g (mol of Fe)$^{-1}$ h^{-1}.
[c] Determined by GC; $\sum C$ signifies the total amounts of oligomers.

Table 7
Ethylene oligomerization with **1b–6b**[a]

Entry	Compound	Cocatalyst	Al/Co	T (°C)	Activity[b]	Oligomer distribution		
						$C_4/\sum C$	$C_6/\sum C$	α-Olefin (%)
1	**1b**	MAO	1000	20	0.14	100		99.0
2	**1b**	MMAO	1000	20	0.22	100		99.0
3	**1b**	Et$_2$AlCl	200	20	3.97	100		97.5
4	**1b**	Et$_2$AlCl	400	30	12.1	99.2	0.8	96.9
5	**1b**	Et$_2$AlCl	600	30	14.1	97.9	2.1	98.5
6	**1b**	Et$_2$AlCl	700	30	16.2	94.9	5.1	96.9
7	**1b**	Et$_2$AlCl	800	30	6.40	100		99.0
8	**1b**	Et$_2$AlCl	900	30	5.79	100		98.5
9	**1b**	Et$_2$AlCl	700	20	4.77	100		98.6
10	**1b**	Et$_2$AlCl	700	40	7.78	93.3	6.7	93.0
11	**1b**	Et$_2$AlCl	700	60	6.92	90.6	9.4	86.6
12	**2b**	Et$_2$AlCl	700	30	11.0	89.7	10.3	90.3
13	**3b**	Et$_2$AlCl	700	30	5.59	92.8	7.2	93.5
14	**4b**	Et$_2$AlCl	700	30	6.81	91.8	8.2	92.3
15	**5b**	Et$_2$AlCl	700	30	17.8	91.9	8.1	92.5
16	**6b**	Et$_2$AlCl	700	30	9.03	95.2	4.8	91.3

Determined by GC; $\sum C$ signifies the total amounts of oligomers.
[a] Reaction conditions: 5 μmol of catalyst; 30 min; 100 mL of toluene.
[b] In units of 10^4 g (mol of Co)$^{-1}$ h^{-1}.

Table 8
Ethylene oligomerization with **1c–6c**[a]

Entry	Complex	Cocatalyst	Al/Ni	T (°C)	Activity[b]	Oligomer distribution[c]		
						$C_4/\sum C$	$C_6/\sum C$	α-Olefin (%)
1	**5c**	MAO	1000	20	0.36	100		98.5
2	**5c**	MMAO	1000	20	0.59	100		94.5
3	**5c**	Et$_2$AlCl	200	20	2.40	97.8	2.2	93.3
4	**5c**	Et$_2$AlCl	100	20	0.39	97.4	2.6	93.7
5	**5c**	Et$_2$AlCl	300	20	3.09	99.0	1.0	95.1
6	**5c**	Et$_2$AlCl	400	20	4.49	97.5	2.5	91.2
7	**5c**	Et$_2$AlCl	500	20	3.42	97.4	2.6	91.4
8	**5c**	Et$_2$AlCl	400	30	17.4	89.7	10.3	48.6
9	**5c**	Et$_2$AlCl	400	40	12.8	97.5	2.5	67.7
10	**5c**	Et$_2$AlCl	400	60	2.15	96.2	3.8	78.9
11	**1c**	Et$_2$AlCl	400	30	12.0	93.1	6.9	75.3
12	**2c**	Et$_2$AlCl	400	30	8.95	94.8	5.2	82.6
13	**3c**	Et$_2$AlCl	400	30	6.29	95.6	4.4	87.2
14	**4c**	Et$_2$AlCl	400	30	3.08	96.9	3.1	91.2
15	**6c**	Et$_2$AlCl	400	30	7.31	95.7	4.3	86.5
16[d]	**5c**	Et$_2$AlCl	400	30	52.0	95.3	3.5	21.4

[a] Reaction conditions: 5 μmol of catalyst; 10 atm of ethylene; 30 min; 100 mL of toluene.
[b] In units of 10^5 g (mol of Ni)$^{-1}$ h^{-1}.
[c] Determined by GC; $\sum C$ signifies the total amounts of oligomers.
[d] 20 equiv. of PPh$_3$.

6b slightly affected the catalytic activities, in which **5b** exhibited better activity than **6b**.

In similar manner, ethylene oligomerization with nickel analogues **1c–6c**/Et$_2$AlCl systems was investigated under the optimum conditions (Al/Ni molar ratio of 400 and 30 °C). Variation of the R^1 group at the *ortho*-positions of the imino-*N* aryl ring resulted in strong influence on the catalytic performance. The increase of steric hindrance of the R^1 group led to

decreasing activity, but higher selectivity of α-olefins (Entries 11–13, Table 8). Furthermore, the complex contained electron-withdrawing substituents on aniline showed lower activity than that with alkyl substituents. For example, complex **4c** showed lower catalytic activity than complexes **1c**, **2c** and **3c**. The similar result was also obtained by complex **6c** comparing with **5c**. In terms of electronic effect, it can be concluded that the introduction of electron-withdrawing groups led to lower

catalytic activity in the nickel-based catalytic system. This is consistent to the simulation results [15] and late transition metal complexes [21]. As observed in the iron catalysts, the nickel complexes containing isopropyl group (in current work) instead of methyl group [12b] perform lower catalytic activities.

Previous studies on nickel-based catalysts have demonstrated that incorporating PPh₃ into catalytic systems led to higher activity and longer catalyst lifetime [9b,12b,22,23]. Therefore, the oligomerization of **5c**/Et₂AlCl was investigated with addition of PPh₃. The addition of 20 equiv. PPh₃ lead to three times higher catalytic activity of 52.0×10^5 g (mol of Ni)$^{-1}$ h^{-1} than that without PPh₃. Moreover, larger amounts of C_6 and C_8 were observed (Entry 17, Table 8). This phenomenon may be attributed to the fact that the active nickel species are coordinated with auxiliary PPh₃, then protected from the impurities in the catalytic reactants.

3. Conclusion

A series of iron (II), cobalt (II) and nickel (II) complexes bearing 2-(1-isopropyl- 2-benzimidazolyl)-6-(1-aryliminoethyl)pyridine ligands have been synthesized, characterized and evaluated as catalyst precursors in ethylene activation. Their results confirm that the increase in net charge of metal center lowers the insertion barrier of ethylene to result in better catalytic activity in ethylene reaction. For all titled complexes, the nature of ligand environments and the reaction parameters, such as different cocatalysts, molar ratio of cocatalyst to metal and reaction temperature, play important roles in influencing the catalytic activity. Upon treatment with MAO or MMAO, the iron (II) complexes showed good catalytic activities for ethylene oligomerization with very high α-olefin selectivity and polymerization for polyethylene wax. Regarding to the catalytic systems of cobalt and nickel complexes, the best suitable cocatalyst is Et₂AlCl. The cobalt catalysts showed considerable to moderate catalytic activities. The nickel catalytic systems enable oligomerization of ethylene to mainly dimmerize for butenes with high activity and moderate to high selectivity of α-olefins. The addition of PPh₃ into the nickel catalytic system can lead to higher catalytic activity.

4. Experimental

4.1. General considerations

All manipulations of air- and moisture-sensitive compounds were carried out under a nitrogen atmosphere using standard Schlenk techniques. Toluene was refluxed over sodium-benzophenone and distilled under nitrogen prior to use. Methylaluminoxane (MAO) was purchased from Albemarle as a 1.46 M solution in toluene. Modified methylaluminoxane (MMAO-3A, 1.93 M in heptane) was purchased from Akzo Corp. Diethylaluminum chloride (Et₂AlCl, 1.70 M in hexane) was purchased from Acros Chemicals. All other reagents were purchased from Aldrich or Acros Chemicals; the boiling range of light petroleum is 60–90 °C and the type of silica gel used is 200–300 mesh. ¹H NMR spectra were recorded on a Bruker DMX 300 MHz instrument at ambient temperature using TMS as an internal standard, while ¹³C NMR spectra were recorded on a Bruker DMX 75 MHz. IR spectra were recorded on a Perkin–Elmer System 2000 FT-IR spectrometer. Elemental analysis was carried out using an HPMOD 1106 microanalyzer. GC analysis was performed with a Carlo Erba Strumentazione gas chromatograph equipped with a flame ionization detector and a 30 m (0.25 mm i.d., 0.25 μm film thickness) DM-1 silica capillary column. The yield of oligomers was calculated by referencing to the mass of the solvent on the basis of the prerequisite that the mass of each fraction was approximately proportional to its integrated area in the GC trace. Selectivity for the linear α-olefin was defined as (amount of linear α-olefin of all fractions)/(total amount of oligomer products) in percent.

4.2. Preparation of the (E)-4-bromo-N-(1-(6-(1-isopropyl-1H-benzo[d]imidazol-2-yl)pyridin-2-yl)ethylidene)-2,6-dimethylbenzenamine (**6**)

In a manner similar to that described for **1–5** [13], the ligand **6** was synthesized as a white solid in 15% yield. M.p.: 170–171 °C. ¹H NMR (300 MHz, CDCl₃, TMS): δ 8.44 (d, 1H, J = 7.9 Hz, Py), 8.39 (d, 1H, J = 7.7 Hz, Py), 7.99 (t, 1H, J = 7.9, 7.7 Hz, Py), 7.86 (m, 1H, Ph), 7.69 (m, 1H, Ph), 7.32 (m, 2H, Ph), 7.23 (s, 2H, Ph), 6.04 (m, 1H, CH), 2.03 (s, 6H, CH₃), 1.76 (d, 6H, J = 6.9 Hz, CH₃). ¹³C NMR (75 MHz, CDCl₃, TMS): δ 167.4, 155.0, 150.1, 147.7, 143.6, 137.7, 134.6, 130.6, 127.8, 127.0, 123.0, 122.4, 121.3, 120.7, 115.8, 113.0, 49.1, 21.5, 17.9, 16.7. IR (KBr disc, cm^{-1}): 2972, 1656, 1570, 1454, 1399, 1204, 853, 823, 771, 749. Anal. Calc. for $C_{25}H_{25}BrN_4$ (461.4): C, 65.08; H, 5.46; N, 12.14. Found: C, 65.28; H, 5.57; N, 11.94%.

4.3. Synthesis of iron complexes **1a–6a**

General procedure: The complexes **1a–6a** were synthesized by the reaction of FeCl₂ · 4H₂O with the corresponding ligands in ethanol. A typical synthetic procedure for complex **1a** can be described as follows. The ligand **1** (382.5 mg, 1.0 mmol) and FeCl₂ · 4H₂O (198.8 mg, 1.0 mmol) were added to a Schlenk tube that was purged three times with nitrogen and then charged with freshly distilled ethanol. The solution turned blue immediately. After the reaction mixture being stirred at room temperature for 12 h, diethyl ether was added to precipitate the complex. The precipitate was filtered, washed with diethyl ether and finally was dried under vacuum to give the pure product as a blue powder in 90% yield. FT-IR (KBr disc, cm^{-1}): 2970, 1593 ($ν_{C=N}$), 1466, 1383, 1212, 1159, 796, 749. Anal. Calc. for $C_{25}H_{26}Cl_2FeN_4$ (509.3): C, 58.96; H, 5.15; N, 11.00. Found: C, 58.86; H, 5.47; N, 10.80%.

Compound **2a** was obtained as a blue powder in 99% yield. FT-IR (KBr disc, cm^{-1}): 2972, 1593 ($\nu_{C=N}$), 1463, 1380, 1212, 1160, 1108, 1014, 814, 792, 754. Anal. Calc. for C$_{27}$H$_{30}$Cl$_2$FeN$_4$ (537.3): C, 60.35; H, 5.63; N, 10.43. Found: C, 59.95; H, 5.73; N, 10.09%.

Compound **3a** was obtained as a blue powder in 95% yield. FT-IR (KBr disc, cm^{-1}): 2965, 1592 ($\nu_{C=N}$), 1462, 1381, 1334, 1161, 1132, 814, 792, 752. Anal. Calc. for C$_{29}$H$_{34}$Cl$_2$FeN$_4$ (565.4): C, 61.61; H, 6.06; N, 9.91. Found: C, 61.59; H, 6.36; N, 9.98%.

Compound **4a** was obtained as a blue powder in 92% yield. FT-IR (KBr disc, cm^{-1}): 2979, 1599 ($\nu_{C=N}$), 1463, 1380, 1336, 1203, 1162, 1132, 844, 787, 750. Anal. Calc. for C$_{23}$H$_{20}$Cl$_4$FeN$_4$ (550.1): C, 50.22; H, 3.66; N, 10.19. Found: C, 50.02; H, 3.36; N, 9.98%.

Compound **5a** was obtained as a blue powder in 99% yield. FT-IR (KBr disc, cm^{-1}): 2974, 1591 ($\nu_{C=N}$), 1462, 1380, 1334, 1217, 1158, 1132, 1014, 814, 751. Anal. Calc. for C$_{26}$H$_{28}$Cl$_2$FeN$_4$ (523.3): C, 59.68; H, 5.39; N, 10.71. Found: C, 59.80; H, 5.44; N, 10.51%.

Compound **6a** was obtained as a blue powder in 80% yield. FT-IR (KBr disc, cm^{-1}): 2970, 1591 ($\nu_{C=N}$), 1465, 1379, 1334, 1214, 1160, 1132, 1016, 812, 748. Anal. Calc. for C$_{25}$H$_{25}$BrCl$_2$FeN$_4$ (588.2): C, 51.05; H, 4.28; N, 9.53. Found: C, 51.00; H, 4.48; N, 9.72%.

4.4. Synthesis of cobalt complexes 1b–6b

General procedure: The cobalt complexes **1b**–**6b** were prepared by the same procedure as for **1a**–**6a** and were obtained as green powder. The synthetic procedure of **1b** can be described as follows. A solution of anhydrous CoCl$_2$ (129.8 mg, 1.0 mmol) in absolute ethanol was added dropwise to the solution of the ligand **1** (382.5 mg, 1.0 mmol) in absolute ethanol. Immediately the color of the solution changed and some green precipitate formed. Then the reaction mixture was stirred at room temperature for 9 h then diluted with diethyl ether. The resulting precipitate was filtered, washed with diethyl ether three times and dried in vacuum. The desired complex was obtained as a green powder in 76% yield. FT-IR (KBr disc, cm^{-1}): 2977, 1593 ($\nu_{C=N}$), 1470, 1407, 1385, 1280, 1214, 1160, 1101, 809, 749. Anal. Calc. for C$_{25}$H$_{26}$Cl$_2$CoN$_4$ (512.3): C, 58.61; H, 5.12; N, 10.94. Found: C, 58.86; H, 5.15; N, 10.84%.

Compound **2b** was isolated as a green powder in 78% yield. FT-IR (KBr disc, cm^{-1}): 2971, 1592 ($\nu_{C=N}$), 1465, 1404, 1378, 1278, 1215, 1163, 1132, 1108, 1021, 789, 749. Anal. Calc. for C$_{27}$H$_{30}$Cl$_2$CoN$_4$ (540.4): C, 60.01; H, 5.60; N, 10.37. Found: C, 59.96; H, 5.56; N, 10.08%.

Compound **3b** was isolated as a green powder in 82% yield. FT-IR (KBr disc, cm^{-1}): 2965, 1591 ($\nu_{C=N}$), 1464, 1405, 1380, 1281, 1163, 1132, 1100, 1018, 793, 752. Anal. Calc. for C$_{29}$H$_{34}$Cl$_2$CoN$_4$ (568.5): C, 61.27; H, 6.03; N, 9.86. Found: C, 59.99; H, 6.07; N, 9.83%.

Compound **4b** was isolated as a green powder in 64% yield. FT-IR (KBr disc, cm^{-1}): 2983, 1591 ($\nu_{C=N}$), 1466, 1434, 1402, 1379, 1276, 1163, 1133, 1097, 1022, 771, 754. Anal. Calc. for C$_{23}$H$_{20}$Cl$_4$CoN$_4$ (553.2): C, 49.94; H, 3.64; N, 10.13. Found: C, 50.09; H, 3.56; N, 10.18%.

Compound **5b** was isolated as a green powder in 74% yield. FT-IR (KBr disc, cm^{-1}): 2974, 1592 ($\nu_{C=N}$), 1464, 1434, 1406, 1380, 1282, 1159, 1132, 1099, 1019, 815, 752. Anal. Calc. for C$_{26}$H$_{28}$Cl$_2$CoN$_4$ (526.4): C, 59.33; H, 5.36; N, 10.64. Found: C, 59.48; H, 5.46; N, 10.76%.

Compound **6b** was isolated as a green powder in 93% yield. FT-IR (KBr disc, cm^{-1}): 2985, 1591 ($\nu_{C=N}$), 1467, 1432, 1405, 1380, 1215, 1161, 1133, 1099, 1019, 814, 749. Anal. Calc. for C$_{25}$H$_{25}$BrCl$_2$CoN$_4$ (591.2): C, 50.79; H, 4.26; N, 9.48. Found: C, 50.65; H, 4.58; N, 9.78%.

4.5. Synthesis of nickel complexes 1c–6c

General procedure: The nickel complexes **1c**–**6c** were also prepared by the same procedure as for **1a**–**6a** and **1b**–**6b**. A typical synthetic procedure of **1c** can be described as follows. A solution of NiCl$_2 \cdot$ 6H$_2$O (237.7 mg, 1.0 mmol) in ethanol was added dropwise to a solution of ligand **1** (382.5 mg, 1.0 mmol) in ethanol at room temperature. The color of the solution changed immediately. The reaction mixture was stirred at room temperature for 10 h then precipitated with diethyl ether. The resulting precipitate was collected, washed with diethyl ether and dried in vacuum. Finally, the objected product was obtained as a yellow powder in 82% yield. FT-IR (KBr disc, cm^{-1}): 2978, 1593 ($\nu_{C=N}$), 1468, 1407, 1335, 1189, 1130, 796, 750. Anal. Calc. for C$_{25}$H$_{26}$Cl$_2$N$_4$Ni (512.1): C, 58.63; H, 5.12; N, 10.94. Found: C, 58.68; H, 5.37; N, 10.76%.

Compound **2c** was isolated as a yellow powder in 98% yield. FT-IR (KBr disc, cm^{-1}): 2973, 1594 ($\nu_{C=N}$), 1467, 1407, 1378, 1279, 1217, 1163, 1133, 1108, 1021, 790, 749. Anal. Calc. for C$_{27}$H$_{30}$Cl$_2$N$_4$Ni (540.2): C, 60.04; H, 5.60; N, 10.37. Found: C, 60.08; H, 5.56; N, 10.21%.

Compound **3c** was isolated as a yellow powder in 93% yield. FT-IR (KBr disc, cm^{-1}): 2966, 1595 ($\nu_{C=N}$), 1467, 1407, 1378, 1156, 1122, 790, 749. Anal. Calc. for C$_{29}$H$_{34}$Cl$_2$N$_4$Ni (568.2): C, 61.30; H, 6.03; N, 9.86. Found: C, 61.18; H, 5.98; N, 9.79%.

Compound **4c** was isolated as a yellow powder in 79% yield. FT-IR (KBr disc, cm^{-1}): 2966, 1593 ($\nu_{C=N}$), 1467, 1406, 1377, 1335, 1228, 1161, 1132, 787, 751. Anal. Calc. for C$_{23}$H$_{20}$Cl$_4$N$_4$Ni (552.9): C, 49.96; H, 3.65; N, 10.13. Found: C, 50.01; H, 3.50; N, 10.05%.

Compound **5c** was isolated as a yellow powder in 94% yield. FT-IR (KBr disc, cm^{-1}): 2977, 1591 ($\nu_{C=N}$), 1466, 1407, 1380, 1335, 1221, 1159, 1134, 813, 751. Anal. Calc. for C$_{26}$H$_{28}$Cl$_2$N$_4$Ni (526.1): C, 59.35; H, 5.36; N, 10.65. Found: C, 59.45; H, 5.40; N, 10.55%.

Compound **6c** was isolated as a yellow powder in 80% yield. FT-IR (KBr disc, cm^{-1}): 2979, 1592 ($\nu_{C=N}$), 1468, 1409, 1382, 1335, 1279, 1217, 1159, 1135, 806, 749. Anal. Calc. for C$_{25}$H$_{25}$BrCl$_2$N$_4$Ni (591.0): C, 50.81; H, 4.26; N, 9.48. Found: C, 50.76; H, 4.50; N, 9.76%.

4.6. Procedure for ethylene oligomerization and polymerization

Ethylene oligomerization and polymerization were performed in a stainless steel autoclave (0.5 L capacity) equipped with a gas ballast through a solenoid clave for continuous feeding of ethylene at constant pressure. A 100 mL amount of toluene containing the catalyst precursor was transferred to the fully dried reactor under a nitrogen atmosphere. The required amount of cocatalyst (MAO, MMAO, or Et$_2$AlCl) was then injected into the reactor via a syringe. At the reaction temperature, the reactor was sealed and pressurized to high ethylene pressure, and the ethylene pressure was maintained with feeding of ethylene. After the reaction mixture was stirred for the desired period, the pressure was released and a small amount of the reaction solution was collected, which was then analyzed by gas chromatography (GC) for determining the composition and mass distribution of oligomers obtained. Then the residual reaction solution was quenched with 5% hydrochloric acid in ethanol. The precipitated low-molecular-weight waxes were collected by fil-

tration, washed with ethanol and water, and dried under vacuum to constant weight.

4.7. X-ray crystallographic studies

All of the crystals of **5a**, **3b**, **5b**, **1c** and **2c** suitable for X-ray diffraction analysis were obtained by laying diethyl ether on a methanol solution at room temperature. With graphite-monochromated Mo Kα radiation ($\lambda = 0.71073$ Å), single-crystal X-ray diffraction studies for **3b**, **1c** and **2c** were carried out on a Bruker SMART 1000 CCD diffractometer, while the intensity data for crystals **5a** and **5b** were collected on a Rigaku RAXIS Rapid IP diffractometer. Cell parameters were obtained by global refinement of the positions of all collected reflections. Intensities were corrected for Lorentz and polarization effects and empirical absorption. The structures of **5a**, **3b**, **5b**, **1c** and **2c** were solved by direct methods and refined by full-matrix least squares on F^2. All non-hydrogen atoms were refined anisotropically. All hydrogen atoms were placed in calculated positions. Structure solution and refinement were performed by using the SHELXL-97 package

Table 9
Crystal data and refinement details for **5a**, **3b**, **5b**, **1c**, and **2c**

	5a	3b	5b	1c	2c
Empirical formula	$C_{26}H_{28}Cl_2FeN_4$	$C_{30}H_{38}Cl_2CoN_4O$	$C_{26}H_{28}Cl_2Co N_4$	$C_{25}H_{26}Cl_2N_4Ni$	$C_{27}H_{30}Cl_2N_4Ni$
Formula weight	523.27	600.47	526.35	512.11	540.16
Crystal color	Blue	Green	Green	Green	Green
Temperature(K)	293(2)	293(2)	293(2)	293(2)	293(2)
Wavelength (Å)	0.71073	0.71073	0.71073	0.71073	0.71073
Crystal system	Orthorhombic	Monoclinic	Orthorhombic	Monoclinic	Triclinic
Space group	$Pca2_1$	$P2_1$	$Pca2_1$	$P2_1/n$	$P\pm$
a (Å)	17.698(4)	9.6001(2)	17.595(4)	11.0385(6)	8.0041(4)
b (Å)	11.800(2)	13.2098(2)	11.824(2)	15.8136(1)	10.9729(6)
c (Å)	24.482(5)	12.5413(2)	24.446(5)	14.3146(8)	15.4537(9)
α (°)	90	90	90	90	82.114(2)
β (°)	90	99.6100(1)	90	107.212(3)	86.097(2)
γ (°)	90	90	90	90	73.549(2)
Volume (Å^3)	5113.1(2)	1568.11(5)	5085.6(2)	2386.8(2)	1288.79(1)
Z	8	2	8	4	2
D_{calc} (Mg m^{-3})	1.360	1.272	1.375	1.425	1.392
μ (mm^{-1})	0.820	0.746	0.906	1.057	0.983
$F(000)$	2176	630	2184	1064	564
Crystal size (mm)	$0.27 \times 0.16 \times 0.06$	$0.26 \times 0.24 \times 0.20$	$0.20 \times 0.18 \times 0.16$	$0.40 \times 0.33 \times 0.30$	$0.33 \times 0.25 \times 0.20$
Limiting indices	$-21 \leqslant h \leqslant 21$, $-14 \leqslant k \leqslant 14$, $-29 \leqslant l \leqslant 28$	$-12 \leqslant h \leqslant 12$, $-17 \leqslant k \leqslant 14$, $-16 \leqslant l \leqslant 16$	$-22 \leqslant h \leqslant 22$, $-15 \leqslant k \leqslant 15$, $-31 \leqslant l \leqslant 31$	$-14 \leqslant h \leqslant 14$, $-19 \leqslant k \leqslant 21$, $-14 \leqslant l \leqslant 19$	$-6 \leqslant h \leqslant 10$, $-14 \leqslant k \leqslant 14$, $-20 \leqslant l \leqslant 20$
Number of reflections collected	27168	17452	36543	23104	16572
Number of unique reflections	8852	6475	11102	5893	6339
R_{int}	0.1121	0.0375	0.0722	0.1664	0.0252
Completeness (%) to (θ)	99.9 (2.07–25.00)	98.7 (1.65–28.30)	99.9 (1.67–27.43)	98.9 (1.97–28.33)	98.3 (1.33–28.35)
Absorption correction	Empirical	Empirical	Empirical	Empirical	Empirical
Data/restraints/parameters	8852/1/596	6475/1/345	11102/1/595	5893/0/290	6339/0/301
Goodness-of-fit on F^2	1.253	1.071	0.847	0.986	1.049
Final R indices [$I > 2\sigma (I)$]	$R_1 = 0.0998$ $wR_2 = 0.2006$	$R_1 = 0.0493$ $wR_2 = 0.1196$	$R_1 = 0.0491$ $wR_2 = 0.0993$	$R_1 = 0.0846$ $wR_2 = 0.1406$	$R_1 = 0.0539$ $wR_2 = 0.1450$
R indices (all data)	$R_1 = 0.1190$ $wR_2 = 0.2087$	$R_1 = 0.0669$ $wR_2 = 0.1292$	$R_1 = 0.1083$ $wR_2 = 0.1119$	$R_1 = 0.2065$ $wR_2 = 0.1823$	$R_1 = 0.0724$ $wR_2 = 0.1661$
Largest difference in peak and hole (e Å^{-3})	0.760 and −0.434	0.378 and −0.202	0.353 and 0.266	0.373 and −0.464	1.556 and −1.151

[24]. Crystal data and processing parameters for **5a**, **3b**, **5b**, **1c** and **2c** are summarized in Table 9.

Acknowledgements

Appendix A. Supplementary material

CCDC 670656, 670657, 670658, 670659 and 670660 contain the supplementary crystallographic data for this paper. These data can be obtained free of charge from The Cambridge Crystallographic Data Centre via www.ccdc.cam.a-c.uk/data_request/cif. Supplementary data associated with this article can be found, in the online version, at doi:10.1016/j.jorganchem.2008.02.007.

References

[1] D. Vogt, in: B. Cornils, W.A. Herrmann (Eds.), Applied Homogeneous Catalysis with Organometallic Compounds, vol. 1, VHC, New York, 1996, pp. 245–258.

[2] J. Skupinska, Chem. Rev. 91 (1991) 613–648.

[3] G.V. Parshall, S.D. Ittel, Homogeneous Catalysis: The Applications and Chemistry of Catalysis by Soluble Transition Metal Complexes, John Wiley and Sons, New York, 1992.

[4] W. Keim, A. Behr, B. Limbäcker, C. Krüger, Angew. Chem., Int. Ed. 22 (1983) 503.

[5] (a) S.D. Ittel, L.K. Johnson, M. Brookhart, Chem. Rev. 100 (2000) 1169–1203;
(b) V.C. Gibson, S.K. Spitzmesser, Chem. Rev. 103 (2003) 283–315;
(c) S. Mecking, Angew. Chem., Int. Ed. 40 (2001) 534–540;
(d) V.C. Gibson, C. Redshaw, G.A. Solan, Chem. Rev. 107 (2007) 1745–1776;
(e) F. Speiser, P. Braustein, L. Saussine, Acc. Chem. Res. 38 (2005) 784–793;
(f) S. Jie, S. Zhang, W.-H. Sun, Petrochem. Tech. (Shiyou Huagong) 35 (2006) 295–300;
(g) W.-H. Sun, D. Zhang, S. Zhang, S. Jie, J. Hou, Kinet. Catal. 47 (2006) 278–283;
(h) W.-H. Sun, S. Zhang, W. Zuo, C.R. Chim. 11 (2008) 307–316.

[6] B.L. Small, M. Brookhart, J. Am. Chem. Soc. 120 (1998) 7143–7144.

[7] G.J.P. Britovsek, M. Bruce, V.C. Gibson, B.S. Kimberley, P.J. Maddox, S. Mastroianni, S.J. McTavish, C. Redshaw, G.A. Solan, S. Strömberg, A.J.P. White, D.J. Williams, J. Am. Chem. Soc. 121 (1999) 8728–8740.

[8] (a) Z. Ma, W.-H. Sun, Z.-L. Li, C.-X. Shao, Y.-L. Hu, X.-H. Li, Polym. Int. 51 (2002) 994–997;
(b) Z. Ma, W.-H. Sun, N. Zhu, Z. Li, C. Shao, Y. Hu, Polym. Int. 51 (2002) 349–352.

[9] (a) W.-H. Sun, S. Jie, S. Zhang, W. Zhang, Y. Song, H. Ma, J. Chen, K. Wedeking, R. Fröhlich, Organometallics 25 (2006) 666–677;
(b) W.-H. Sun, S. Zhang, S. Jie, W. Zhang, Y. Li, H. Ma, J. Chen, K. Wedeking, R. Fröhlich, J. Organomet. Chem. 691 (2006) 4196–4203;

(c) S. Jie, S. Zhang, K. Wedeking, W. Zhang, H. Ma, X. Lu, Y. Deng, W.-H. Sun, C.R. Chim. 9 (2006) 1500–1509;
(d) S. Jie, S. Zhang, W.-H. Sun, X. Kuang, T. Liu, J. Guo, J. Mol. Catal. A: Chem. 269 (2007) 85–96;
(e) L. Wang, W.-H. Sun, L. Han, H. Yang, Y. Hu, X. Jin, J. Organomet. Chem. 658 (2002) 62–70;
(f) M. Zhang, S. Zhang, P. Hao, S. Jie, W.-H. Sun, P. Li, X. Lu, Eur. J. Inorg. Chem. (2007) 3816–3826;
(g) M. Zhang, P. Hao, W. Zuo, S. Jie, W.-H. Sun, J. Organomet. Chem. 693 (2008) 483–491.

[10] W.-H. Sun, K. Wang, K. Wedeking, D. Zhang, S. Zhang, J. Cai, Y. Li, Organometallics 26 (2007) 4781–4790.

[11] (a) S. Adewuyi, G. Li, S. Zhang, W. Wang, P. Hao, W.-H. Sun, N. Tang, J. Yi, J. Organomet. Chem. 692 (2007) 3532–3541;
(b) W.-H. Sun, P. Hao, G. Li, S. Zhang, W. Wang, J. Yi, M. Asma, N. Tang, J. Organomet. Chem. 692 (2007) 4506–4518.

[12] (a) W.-H. Sun, P. Hao, S. Zhang, Q. Shi, W. Zuo, X. Tang, Organometallics 26 (2007) 2720–2734;
(b) P. Hao, S. Zhang, W.-H. Sun, Q. Shi, S. Adewuyi, X. Lu, P. Li, Organometallics 26 (2007) 2439–2446.

[13] Y. Chen, W. Zuo, P. Hao, S. Zhang, K. Gao, W.-H. Sun, J. Organomet. Chem. 693 (2008) 750–762.

[14] (a) P.J. Flory, J. Am. Chem. Soc. 62 (1940) 1561–1565;
(b) G.V. Schulz, Z. Phys. Chem., Abt. B 30 (1935) 379–398;
(c) G.V. Schulz, Z. Phys. Chem., Abt. B 43 (1939) 25–46;
(d) M.V. Meurs, G.J.P. Britovsek, V.C. Gibson, S.A. Cohen, J. Am. Chem. Soc. 127 (2005) 9913–9923;
(e) G.J.P. Britovsek, S.A. Cohen, V.C. Gibson, M.V. Meurs, J. Am. Chem. Soc. 126 (2004) 10701–10702.

[15] T. Zhang, D. Guo, S. Jie, W.-H. Sun, T. Li, X. Yang, J. Polym. Sci. A: Polym. Chem. 42 (2004) 4765–4774.

[16] T. Zhang, W.-H. Sun, T. Li, X. Yang, J. Mol. Catal. A: Chem. 218 (2004) 119–124.

[17] N.J. Robertson, M.J. Carney, J.A. Halfen, Inorg. Chem. 42 (2003) 6876–6885.

[18] G.J.P. Britovsek, S. Mastroianni, G.A. Solan, S.P.D. Baugh, C. Redshaw, V.C. Gibson, A.J.P. White, D.J. Williams, M.R.J. Elsegood, Chem. Eur. J. 6 (2000) 2221–2231.

[19] (a) C. Bianchini, G. Mantovani, A. Meli, F. Migliacci, F. Zanobini, F. Laschi, A. Sommazzi, Eur. J. Inorg. Chem. 8 (2003) 1620–1631;
(b) Y. Chen, C. Qian, J. Sun, Organometallics 22 (2003) 1231–1236;
(c) Y. Chen, R. Chen, C. Qian, X. Dong, J. Sun, Organometallics 22 (2003) 4312–4321.

[20] J.D.A. Pelletier, Y.D.M. Champouret, J. Cadarso, L. Clowes, M. Gañete, K. Singh, V. Thanarajasingham, G.A. Solan, J. Organomet. Chem. 691 (2006) 4114–4123.

[21] D. Guo, L. Han, T. Zhang, W. Sun, T. Yang, Macromol. Theory Simul. 11 (2002) 1006–1012.

[22] (a) C. Carlini, M. Isola, V. Liuzzo, A.M.R. Galletti, G. Sbrana, Appl. Catal. A: Gen. 231 (2002) 307–320;
(b) J.C. Jenkins, M. Brookhart, Organometallics 22 (2003) 250–256.

[23] W.-H. Sun, W. Zhang, T. Gao, X. Tang, L. Chen, Y. Li, X. Jin, J. Organomet. Chem. 689 (2004) 917–929.

[24] G.M. Sheldrick, SHELXTL-97, Program for the Refinement of Crystal Structures, University of Gottingen, Germany, 1997.